Physics in Medicine & Biology

IPEM Institute of Physics and Engineering in Medicine

ACCEPTED MANUSCRIPT • OPEN ACCESS

Auto-commissioning of a Monte Carlo electron beam model with application to photon MLC shaped electron fields

To cite this article before publication: Michael K Fix *et al* 2023 *Phys. Med. Biol.* in press https://doi.org/10.1088/1361-6560/acb755

Auto-commissioning of a Monte Carlo electron beam model with application to photon MLC shaped electron fields

M.K. Fix, D. Frei, S. Mueller, G. Guyer, H.A. Loebner, W. Volken and P. Manser

Division of Medical Radiation Physics and Department of Radiation Oncology, Inselspital, Bern University Hospital, and University of Bern, Bern, Switzerland

To be submitted as a research article to the Physics in Medicine & Biology special issue: Focus on the Monte Carlo Method for Medical Applications: From Macro to Microscale

Corresponding Author:

Michael K. Fix, PhD

Division of Medical Radiation Physics

Inselspital – University Hospital Bern

CH-3010 Bern

Switzerland

Tel: +41 31 632 2119

E-Mail: michael.fix@insel.ch

Abstract

Objective: Presently electron beam treatments are delivered using dedicated applicators. An alternative is the usage of the already installed photon multileaf collimator (pMLC) enabling efficient electron treatments. Currently, the commissioning of beam models is a manual and time-consuming process. In this work an auto-commissioning procedure for the Monte Carlo (MC) beam model part representing the beam above the pMLC is developed for TrueBeam systems with electron energies from 6 to 22 MeV.

Approach: The analytical part of the electron beam model includes a main source representing the primary beam and a jaw source representing the head scatter contribution each consisting of an electron and a photon component, while MC radiation transport is performed for the pMLC. The auto-commissioning of this analytical part relies on information pre-determined from MC simulations, in-air dose profiles and absolute dose measurements in water for different field sizes and source to surface distances (SSDs). For validation calculated and measured dose distributions in water were compared for different field sizes, SSDs and beam energies for eight TrueBeam systems. Furthermore, a sternum case in an anthropomorphic phantom was considered and calculated and measured dose distributions were compared at different SSDs.

Main Results: Instead of the manual commissioning taking up to several days of calculation time and several hours of user time, the auto-commissioning is carried out in a few minutes. Measured and calculated dose distributions agree generally within 3% of maximum dose or 2 mm. The gamma passing rates for the sternum case ranged from 96% to 99% (3% (global)/2 mm criteria, 10% threshold).

Significance: The auto-commissioning procedure was successfully implemented and applied to eight TrueBeam systems. The newly developed user-friendly auto-commissioning procedure allows an efficient commissioning of an MC electron beam model and eases the usage of advanced electron radiotherapy utilizing the pMLC for beam shaping.

Keywords: Electron radiotherapy, Monte Carlo, beam modelling, dose calculation

1. Introduction

Over the last few decades, an enormous effort was made to replace patient-specific blocks in photon radiotherapy with a photon multileaf collimator (pMLC). Initially, the pMLC substantially improved treatment efficiency and safety (Brewster *et al.*, 1995; Boyer *et al.*, 2001). Along with such new hardware, expansions of new treatment planning capabilities like inverse treatment planning were accomplished. These further enabled the development of dynamic delivery techniques like intensity modulated radiotherapy (IMRT) or volumetric modulated arc therapy (VMAT), which both are current state-of-the-art delivery techniques in photon radiotherapy (Convery and Rosenbloom, 1992; Bortfeld *et al.*, 1994; Yu, 1995; Otto, 2008). More recently new delivery techniques including even more degrees of freedom such as dynamic trajectory radiotherapy (DTRT) (Fix *et al.*, 2018; Guyer *et al.*, 2022) were proposed (Smyth *et al.*, 2019). However, a similar effort was not made for electron radiotherapy. Standard electron treatments are still applied using the cumbersome and inefficient standard or molded patient-specific cut-out placed in dedicated electron applicators for which limited planning features are available (Klein *et al.*, 2008). The usage of standard electron treatments needs effort in commissioning and maintenance for each energy-applicator combination and the fabrication of cut-outs including toxic materials (Fix *et al.*, 2013; Skinner *et al.*, 2019). Furthermore, combined photon and electron treatments have to be interrupted to mount and dismount the heavy add-on applicators (Henzen *et al.*, 2014b). In addition, treatment errors due to accidentally using a wrong cut-out are a potential risk (Mueller *et al.*, 2018a). All these issues negatively affect the workflow in clinical routine and make intensity and energy modulation of electron beams virtually unrealizable. Thus, the potential of electron radiotherapy is not yet utilized, although their sharp distal dose fall-off in tissue provides fundamentally different characteristics compared with photon beam dose distributions. This characteristic makes electron beams suitable for treatments of superficial targets. In research institutions the potential of electron beam dose characteristics was investigated by means of inverse planning based advanced techniques. These techniques include modulated electron radiotherapy (MERT) using either a few leaf electron collimator (Al-Yahya *et al.*, 2005; Al-Yahya *et*

al., 2007; Alexander *et al.*, 2010; Eldib *et al.*, 2013), a dedicated add-on electron MLC (Engel and Gauer, 2009; Vatanen *et al.*, 2009; Gauer *et al.*, 2010; O'Shea *et al.*, 2011b; Jin *et al.*, 2014) or the pMLC (du Plessis *et al.*, 2006; Jin *et al.*, 2008; Klein *et al.*, 2008; Klein *et al.*, 2009; Salguero *et al.*, 2009; Salguero *et al.*, 2010; Mihaljevic *et al.*, 2011; Henzen *et al.*, 2014c; Henzen *et al.*, 2014a; Lloyd *et al.*, 2016; Kaluarachchi *et al.*, 2020). Using pMLC based collimation devices for electron beams offers great advantages with respect to the above-mentioned limitations for current standard electron treatments. The usage of the pMLC has the additional benefit that the pMLC is already part of the treatment unit head. Thus, no additional add-on hardware has to be mounted or dismounted, which improves safety, reduces workload for radiation therapy technologists and avoids gantry sag due to the weight of an electron beam add-on device. Using the pMLC for electron beams is also valuable for the treatment workflow, specifically for advanced treatment techniques such as MERT, mixed beam radiotherapy (MBRT) (Klein *et al.*, 2008; Surucu *et al.*, 2010; Ge and Faddegon, 2011; Palma *et al.*, 2012; Renaud *et al.*, 2017, 2019; Heng *et al.*, 2021; Mueller *et al.*, 2022) or dynamic mixed beam radiotherapy (Mueller *et al.*, 2018b).

Using a Monte Carlo (MC) based beam model and dose calculation for predicting the dose distribution of electron beams in radiotherapy is well established and available in commercial products for standard electron beam applications (Cygler *et al.*, 2004; Cygler *et al.*, 2005; Ding *et al.*, 2005; Ding *et al.*, 2006; Pemler *et al.*, 2006; Popple *et al.*, 2006; Fragoso *et al.*, 2008; Edimo *et al.*, 2009; Ali *et al.*, 2011; Ojala *et al.*, 2016; Huang *et al.*, 2019; Snyder *et al.*, 2019). In order to apply electron beams with field sizes shaped by the pMLC, the currently used beam models in treatment planning systems for applicator-based electron beam delivery are not appropriate. Instead of the applicator, the pMLC has to be considered in the beam model. Furthermore, a commissioning procedure for such a beam model is an essential requirement for widespread use. Currently, such procedures are performed mainly manually and typically in an iterative manner including substantial computational resources and many user interactions (Leal *et al.*, 2004; Jin *et al.*, 2008; Klein *et al.*, 2008; Mihaljevic *et al.*, 2011; Henzen *et al.*, 2014c; Lloyd *et al.*, 2016; Mueller *et al.*, 2018a; Kaluarachchi *et al.*, 2020). An automated commissioning was presented by Henzen *et al.* (2014c)

applied for a single Clinac and a single TrueBeam system for different field sizes at a source to surface distance (SSD) of 70 cm. However, this commissioning procedure is limited to a sub-set of beam model parameters, which are not sufficient for a larger range of SSDs and TrueBeam systems. Therefore, manual commissioning steps have to be performed for the remaining beam model parameter. Hence, the currently applied approaches are time consuming meaning the commissioning takes up to several days. In addition, dedicated MC expertise as well as a detailed knowledge of the beam model are needed. In this work a fast (i.e. ~ minutes) and user-friendly auto-commissioning process of the beam model part representing the beam above the pMLC was developed for TrueBeam systems (Varian Medical Systems, Palo Alto, CA) using the pMLC for shaping the electron fields and electron energies ranging from 6 to 22 MeV. This auto-commissioning was then validated for eight different TrueBeam systems.

2. Methods

The development of the proposed auto-commissioning procedure for the beam model part representing the beam above the pMLC consists of different parts illustrated in Figure 1 and described in detail in this section. First the beam model itself including the sampling procedure is described (cf. section 2.1). Next information of the MC simulations performed using EGSnrc (cf. section 2.2.1) and simulations using the electron MC (eMC) algorithm eMC-2020 (cf. sections 2.2.2 and 2.5) are provided. These MC simulations include the pre-determined information to be performed only once, meaning the resulting data is used for all TrueBeam systems. Finally, the descriptions of necessary measurements of a specific TrueBeam system (cf. section 2.3) and the auto-commissioning (cf. section 2.4), which determines the tunable parameters of the beam model, are provided.

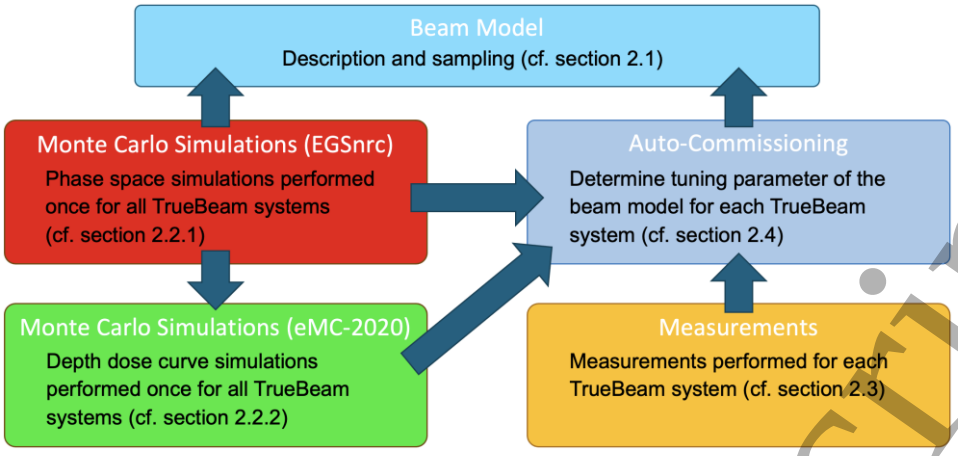

Figure 1. Overview of different parts of the proposed procedure. The arrows indicate which part provides input information for other parts in the procedure. (eMC-2020 refers to the electron MC algorithm described in section 2.5)

2.1. Electron beam model

In this section the beam model and the corresponding sampling procedure is described. A schematic view is depicted in Figure 2.

2.1.1. Beam model

The beam model considered in this work is based on the beam model described in Henzen *et al.* (2014c). The beam defining components of the accelerator are illustrated in Figure 2, which are represented by the two sources in the analytical part and the pMLC as the patient specific component for which MC radiation transport is performed.

The primary electrons and bremsstrahlung photons are characterized by a main source with a focus *f* located closely to the scattering foil system in the linear accelerator head of a TrueBeam system. In addition, the main source (electrons and photons) is associated with a two-dimensional lateral Gaussian shaped intensity origin distribution with a standard deviation σ_f. To determine the initial direction of the source particle, a fluence distribution in a plane typically located at an SSD of 70 or 75 cm, referred to as sampling plane in Figure 2, is related to this source. In addition, an electron and photon energy spectrum are assigned to the main source. The scattered electrons and photons of all components in the treatment head except the scattering foil are associated with the jaw source, which consists of four sub-sources linked to the four secondary collimator jaws. The secondary collimator jaws are set to a patient independent static field size of 15 x 35 cm^2 for

accelerators equipped with a Millennium 120 pMLC (M120), while this field size is reduced to 15 x 17 cm^2 in the case where the high-definition pMLC (HDMLC) is used. These settings remain the same for all electron beam energies. Each sub-source defines a line source for electrons and photons similar to the line source defined in a previous publication for applicator-based electron radiotherapy (Fix *et al.*, 2013). The origin distribution is represented by a horizontal line on the inner side of the jaw for which the width corresponds to the jaw setting of the corresponding field size. Similar to the main source, a fluence distribution in the sampling plane is used to determine the initial direction of the source particle. Furthermore, an electron and photon energy spectrum are associated with the line source. Finally, a sampling procedure for the beam model is defined to provide a particle for the dose calculation algorithm in the beam reconstruction plane (Figure 2).

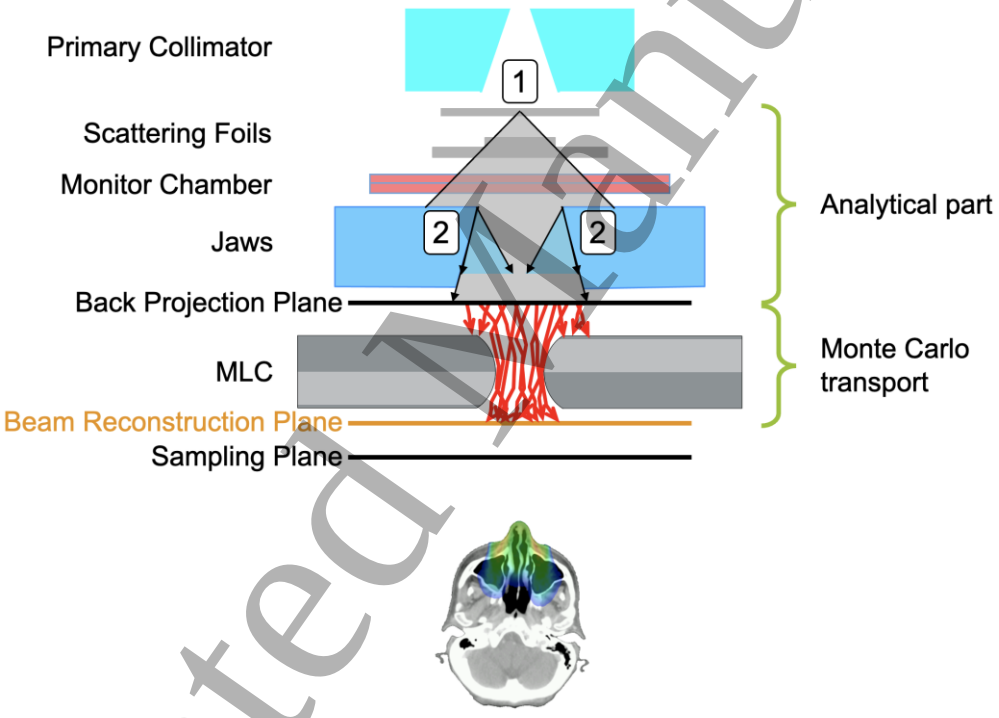

Figure 2. Schematic view of the proposed beam model and dose calculation algorithm. The beam model consists of a patient independent analytical part ([1] = main source and [2] = jaw source) followed by a patient specific Monte Carlo radiation transport layer. The beam model reconstructs the electron beam of a specific beam energy in the beam reconstruction plane starting from a sampling plane followed by a dedicated back projection algorithm to the back projection plane from where the Monte Carlo transport is applied. The particles are then provided for the dose calculation algorithm for which the electron Monte Carlo is used (cf. section 2.5).

2.1.2. Sampling procedure

The sampling procedure applied for the beam model reconstructs the radiation beam in the beam reconstruction plane (Figure 2) and consists of the following steps:

1. Sample the sub-source.
2. Sample a point in the beam sampling plane from the two-dimensional fluence distribution for the sub-source determined in step 1.
3. Sample the energy from the energy distribution for the sub-source determined in step 1.
4. Determine the initial direction by connecting the point in the beam sampling plane (step 2) with a sampled point from the origin distribution for the sub-source determined in step 1.
5. In case of a photon particle, ray-tracing is applied to determine if the photon hits the jaws. In case the photon hits the jaws, the photon is rejected. Otherwise, the location in the back projection plane (Figure 2) is determined by ray-tracing.
6. In case of an electron particle, the initial direction of the electron determined in step 4 is corrected in order to account for the in-air scatter along the path from the origin to the sampling plane. The correction values for the direction cosines u and v for the electron is sampled form a Gaussian distribution with an energy E dependent standard deviation $\sigma_\theta(E)$, which is determined using the Highland approximation for in-air scatter corrections (Lynch and Dahl, 1991). At this stage the sampling of the starting point does not take into account the impact of the jaws. The impact of the jaws is corrected by back projecting the electrons to the plane of the jaws. This procedure was described in Fix *et al.* (2010; 2013) except that in this work the Highland approximation for in-air scatter is used. With this procedure it is determined whether or not the electron passes through the opening of the jaws. The electron is rejected if it does not pass through the opening of the jaws. Otherwise, the electron is projected to the back projection plane.
7. For the non-rejected particle, MC radiation transport through the pMLC starts in the back projection plane downstream to the beam reconstruction plane. In case the particle or all potentially created secondary particles reach this plane, they are passed on to the dose calculation algorithm.

Thus, for the commissioning procedure of the proposed beam model representing the analytical part the following parameters have to be determined for the specific electron beam energy: For the main electron and photon source the focus position, the focus size, the fluence distribution and the energy

spectrum in the sampling plane and for the jaw source or more specifically for each of the four electron and photon sub-sources the origin distribution as well as the fluence distribution and energy spectrum in the sampling plane. In addition, the weight of each individual sub-source has to be determined.

2.2. Pre-determined MC simulations

In this work, the auto-commissioning of the beam model for a specific treatment unit of a TrueBeam system is performed based on a sampling plane at an SSD of 70 or 75 cm, which does not have to coincide with the beam reconstruction plane expected to be closer to the pMLC. The secondary collimator jaws are set to a static field of 15 x 35 cm^2 or 15 x 17 cm^2 when the TrueBeam system is equipped with the M120 or the HDMLC, respectively. For these settings pre-calculated information is determined by MC simulations for a treatment unit in general, that is independent of a specific linear accelerator instance, and described in the following sections.

2.2.1. MC simulation using EGSnrc

This part consists of full MC simulations using EGSnrc as the transport code (version 2020) (Kawrakow and Rogers, 2002). For these simulations BEAMnrc (Rogers *et al.*, 1995) was applied to model the beam defining components including the primary collimator, the scattering foil system, the monitor chamber, the secondary collimator jaws and the reticle for the different electron beam energies. The input is based on confidential information from Varian Medical System (Palo Alto, CA) for Clinac linear accelerators together with physical measurements on scattering foils performed, which is considered to be suitable to represent a TrueBeam system for the purpose of this work and supported by the work of Lloyd *et al.* (2015). During these simulations, phase space files in the sampling planes at SSD = 70 and 75 cm for the maximal field size possible (40 x 40 cm^2), and the field size used for the beam model were generated. These phase space files were analyzed in order to determine radiation beam characteristics. One aspect of the phase space file analyses was the particle fluence referred as fluence in the following. For this purpose, all particles (electrons and photons) from the scattering foil system were initially assigned to the main source. However, if the particle interacts in one of the secondary collimator jaws, they were re-assigned to the jaw source of the

corresponding collimator jaw. For the purpose of particle assignment to a source, the particle history was scored during the MC simulation and accordingly stored in the phase space file. During the evaluation of the phase space file, the particles can then be sorted according to the different sources considered. This is especially important as the contributions of the different sources cannot be separated in the measurement data, but are needed for the auto-commissioning.

In addition to the fluence in the sampling plane, also the origin distribution for the jaw source was analyzed based on the phase space files. As mentioned above, the origin distribution for each jaw sub-source is a line located on the beam shaping surface of each jaw. While the true origin distribution covers the complete surface along the beam direction, this distribution is not homogeneous and the line determined represents the average value of the extracted distribution from the phase space files.

Apart from the determination of the fluence also the energy spectrum of each photon source (main and jaw) was extracted from the phase space file for each electron beam energy.

Finally, the depth dose curve for the jaw sources was calculated by performing MC simulations using DOSXYZnrc with the corresponding particles from the phase space files as input. All these simulations were performed for each electron beam energy considered, namely 6, 9, 12, 15, 16, 18, 20 and 22 MeV.

In summary, this part provides the following input to the eMC-2020 simulations (cf. section 2.2.2), the auto-commissioning (cf. section 2.4) as well as the beam model (cf. Figure 1):

- Electron fluence of the jaw source used in the eMC-2020 simulations, the auto-commissioning as well as the beam model
- Photon fluence of the main and jaw source used in the eMC-2020 simulations, the auto-commissioning as well as the beam model
- Origin distribution of the jaw source used in the eMC-2020 simulations and the beam model
- Photon energy distributions of the main and jaw source used in the eMC-2020 simulations and the beam model

- Depth dose curve in water of the jaw source used in the auto-commissioning

2.2.2. Simulation using eMC-2020

In addition to the MC simulation described in the previous section, additional depth dose calculations are needed for the auto-commissioning using the identical dose calculation algorithm as for which the beam model is commissioned. In this study the electron MC (eMC) algorithm eMC-2020 (cf. section 2.5) is used. This guarantees the reproducibility of calculated dose distributions when using the commissioned beam model in conjunction with eMC-2020. In total four different sets of depth dose curves were calculated, namely for:

- mono-energetic electrons of the main electron source
- mono-energetic electrons of the jaw electron source
- the main photon source using the energy spectrum from the EGSnrc simulation
- the jaw photon source using the energy spectrum form the EGSnrc simulation

Thereby for the main sources the calculations were performed for different locations of the focus *f* of the main source at distances of 6, 8, 10, 12 and 14 cm from the upper surface of the photon bremsstrahlung target being the typically used origin of the central beam axis. In addition, for each focus position *f* different σ_f values of 0.0, 0.5, 1.0, 1.5 and 2.0 cm were considered. For all the four above mentioned sets of depth dose calculations the following situations were included: field sizes of 15 x 35 cm^2 and 15 x 17 cm^2, SSD1 = sampling plane (70 or 75 cm) and SSD2 = 90 cm, pMLC shaped field sizes of 2 x 2 cm^2, 5 x 5 cm^2 and fully retracted pMLC leaves.

2.3. Measurements

In order to perform the auto-commissioning a set of dose measurements are needed to determine the tuning parameters of the beam model. For the proposed auto-commissioning procedure, the following set of measurements for each electron beam energy are required:

- relative in-air dose profiles in crossline and inline directions with the pMLC fully retracted for a field size of 40 x 40 cm^2 at SSD1

- depth dose curves in water at SSD1 and SSD2 in units of cGy/MU with the pMLC fully retracted and field sizes of either 15 x 35 cm^2 or 15 x 17 cm^2 depending on the pMLC type available
- depth dose curves in water at SSD1 in units of cGy/MU and pMLC shaped field sizes of 5 x 5 cm^2 and 2 x 2 cm^2

The complete set of commissioning measurements were performed for in total eight TrueBeam systems with seven TrueBeam systems equipped with a M120 and one TrueBeam system equipped with an HDMLC. Thereby, the electron beam energy ranges from 6 to 22 MeV. Table 1 summarizes the data available.

Table 1. Overview of the TrueBeam systems including the set of electron beam energies, for which a complete commissioning data set together with additional validation measurements were available. The last column provides information of the water tank and detector (field & reference detector) equipment used for the measurements (mD = microDiamond; SF = Semiflex 31010; D = diode TW60017; E = EDGE-Detector).

TB-System	6 MeV	9 MeV	12 MeV	15 MeV	16 MeV	18 MeV	20 MeV	22 MeV	measurement equipment used
Millennium-1	X	X	X	X		X		X	MP3 mD & SF
Millennium-2	X	X	X	X		X		X	BEAMSCAN mD & SF
Millennium-3	X	X	X	X		X		X	BEAMSCAN mD & SF
Millennium-4	X	X	X	X		X			MP3 mD & SF
Millennium-5	X	X	X	X		X			MP3 mD & SF
Millennium-6	X	X	X	X		X			BEAMSCAN mD & SF
Millennium-7		X	X		X		X		3D Scanner D & E
HDMLC-1	X	X	X		X		X		BEAMSCAN mD & SF

These measurements were performed using a MP3, a BEAMSCAN (both PTW Freiburg, Germany) or a 3D Scanner (Sun Nuclear , Melbourne, FL) water tank. For the two PTW water tanks a microDiamond and a Semiflex 31010 (both PTW, Freiburg, Germany) were used as field detector and reference detector, respectively. In case of the 3D scanner water tank a diode detector TW60017

(PTW, Freiburg, Germany) and an EDGE-Detector (Sun Nuclear, Melbourne, FL) was used as field detector and reference detector, respectively.

2.4. Auto-commissioning

The auto-commissioning procedure is illustrated in Figure 3:

1. The first step in the auto-commissioning part is to construct a two-dimensional fluence distribution for the main electron source. For this purpose, the measured in-air profiles in crossline and inline direction at SSD1 using a 40 x 40 cm^2 field size (at iso-center) are used. The corresponding contribution from electrons from the secondary collimator jaws as determined by MC simulations using EGSnrc (cf. Figure 2) are subtracted from these measured in-air profiles. This results in measured fluence profiles for the main electron source p_x and p_y in crossline and inline direction. The two-dimensional fluence distribution $f_{main_{e^-}}$ for the electrons of the main source is then determined by the following equation:

$$f_{main_{e^-}} = \frac{p_x(r)+p_x(-r)+p_y(r)+p_y(-r)}{4} \quad (1)$$

   For the photons of the main source the fluence distribution as determined by the EGSnrc MC simulation is used.
2. In the next step, the measured depth dose contribution from the main source (electrons and photons) at SSD1 is extracted. This is done by subtracting the pre-calculated jaw source depth dose curve using EGSnrc MC simulations from the measured depth dose curve. In this step the depth dose contribution from the jaws is multiplied by a jaw-fraction factor with values of 1, 2, 4, 6, 8 or 10% of the measured depth dose curve around the maximum dose.
3. Then the measured depth dose contribution from the main source is de-convolved with the corresponding pre-calculated depth dose curves for mono-energetic electrons and the photon depth dose curve for the main source. This results in the energy spectrum of the electrons of the main source as well as the source weight of the photons of the main source.
4. Now the contribution to the depth dose curve in water of the electrons and photons from the main source can be calculated at SSD1.

5. The depth dose curve contribution determined in step 4 is now subtracted from the measured depth dose curve leading to the measured depth dose associated with the jaw source.
6. Similar to step 3 the resulting measured depth dose curve from step 5 is de-convolved with the corresponding pre-calculated depth dose curves for mono-energetic electrons and the photon depth dose curve for the jaw source. In addition, the source weight of the photons of the jaw source is obtained.
7. Now all parameters are determined in order to calculate the total depth dose curve in water at SSD2 with the pMLC fully retracted.
8. Steps 3 to 7 are repeated for each location of the focus *f* of the main source. These depth dose curves as a function of the focus *f* are now compared with the corresponding measured depth dose curve at SSD2. Interpolation of the focus location *f* to match this measured depth dose curve is performed to determine the final focus *f* of the main source for a given σ_f and jaw-fraction.
9. Now all steps from 3 to 6 are repeated for each value of σ_f. Then the depth dose curves in water at SSD1 for an pMLC shaped field size of 2 x 2 cm^2 are calculated. These depth dose curves as a function of σ_f are now compared with the corresponding measured depth dose curve. Interpolation of σ_f to match this measured depth dose curve is performed to determine the final value for σ_f of the main source for a given jaw-fraction.
10. Next all steps from 2 to 9 are repeated for each value of jaw-fraction and the depth dose curves in water at SSD1 for an pMLC shaped field size of 5 x 5 cm^2 are calculated. These depth dose curves as a function of jaw-fraction are now compared with the corresponding measured depth dose curve. Interpolation of the jaw-fraction to match this measured depth dose curve is performed to determine the final value for the jaw-fraction.

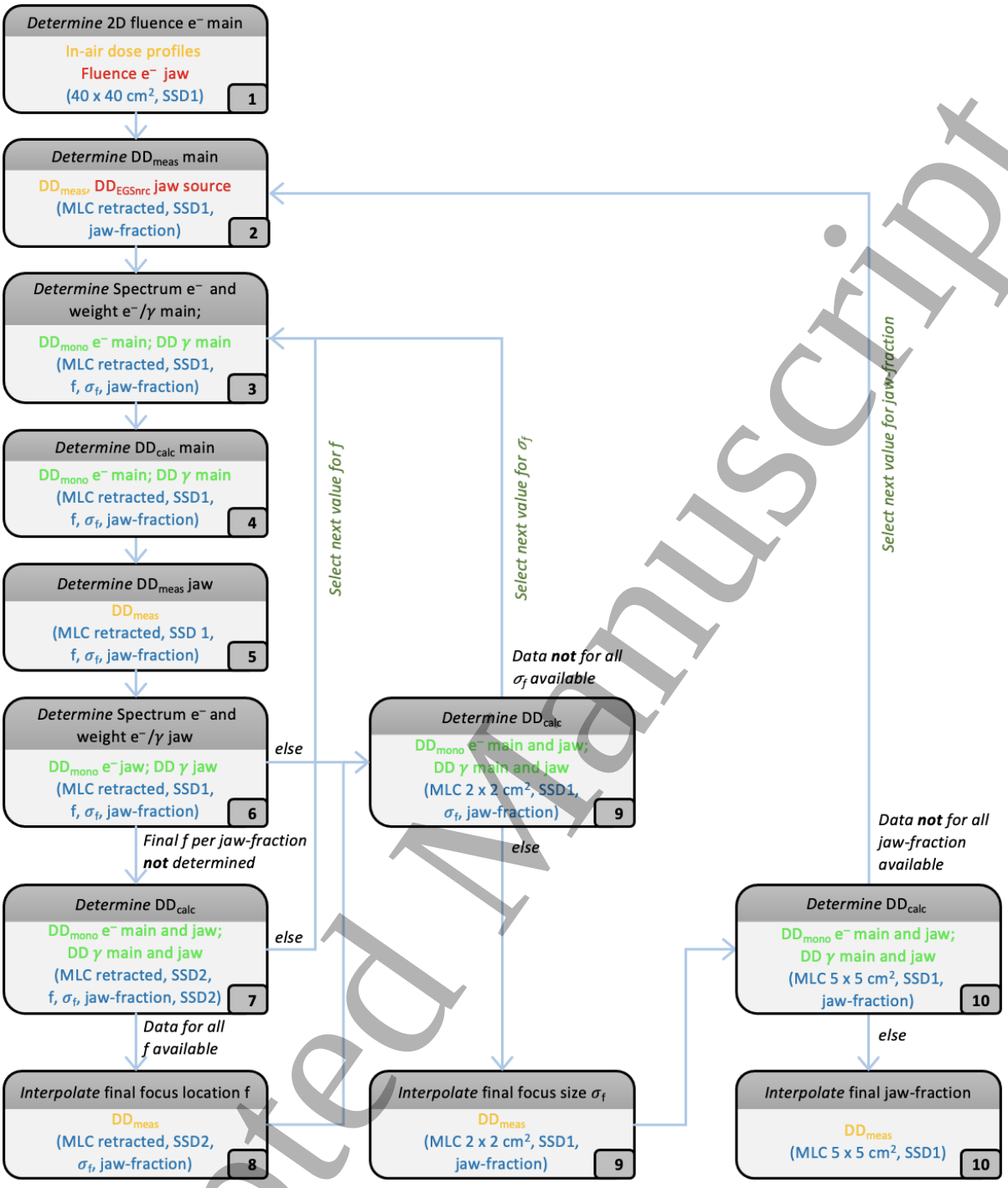

Figure 3. Flow chart of the auto-commissioning procedure. The different steps (1 to 10) are described in the text. The upper part (dark grey) in the rectangles illustrates what is performed in the step, while the lower part indicates the input used for the step. The source of the input data shown is additionally indicated by different colours: yellow refers to measured data, red refers to pre-calculated data based in EGSnrc Monte Carlo simulations, green refers to pre-calculated data based on eMC-2020 (cf. section 2.5) and blue indicates specific settings for the MLC and SSD as well as for the used beam model parameters in the step. (DD = depth dose; f = focus position of the main source; σ_f = focus size of the main source; main and jaw refer to the main source and jaw source, respectively)

After the completion of the ten steps all parameters of the beam model are determined and the commissioning procedure is fully completed.

During the auto-commissioning the focus position f and the standard deviation σ_f of the main source associated with the spot size are determined in step 8 and 9. Both parameters are determined independently from each other. This is possible as these parameters are established by means of different measurements and the depth dose curve for the field size with fully retracted pMLC is virtually independent on the spot size, hence the corresponding measured depth dose curve at SSD = 90 cm can be used to determine the position of the focus. Given the position of the focus the depth dose curve for the pMLC shaped field size of 2 x 2 cm^2 is then used to determine the value for σ_f.

2.5. Dose calculation

The fully commissioned beam model provides the particles in the beam reconstruction plane for the dose calculation algorithm (cf. Figure 2). The dose calculation performed in this work is based on the eMC algorithm for both pre-determined MC simulations and validation (Neuenschwander and Born, 1992; Fix *et al.*, 2013). Compared to the previously used version of this dose calculation algorithm, a new version was used for this study, referred to as eMC-2020, which includes improvements recently developed for this work. This version is based on local simulations performed with the more recent EGSnrc version 2020 (Kawrakow and Rogers, 2002). In this context not only the program language was changed from Mortran to C++ for the simulation framework using the advanced application in egs++ to generate the database for eMC-2020 in the local simulation, but also improvements in the macro simulation were included. Mainly the following improvements were implemented in the version of eMC-2020 used in this work, for which some more detailed information about these improvements is provided in the appendix:

1. The correlation between energy and direction of secondary particles was taken into account. Hence, the generation of the database was modified to score the data needed for such a correlated sampling.

2. The energy deposition of the primary electron was modified. The new version takes the small build-up effect occurring in the spheres into account and thus improves the energy deposition distribution of the local simulation in the macro step compared with the previous versions.
3. Lung with density 0.1 g/cm^3 (lung light) was included in the database as an additional sampling material between air and lung with density 0.3 g/cm^3.
4. Dedicated and efficient air transport.

The statistical uncertainty of the MC calculated dose distributions was less than 1% (one std. dev.).

2.6. Validation

As a first test of the completely commissioned beam model calculations of the dose distributions for those situations used during the commissioning are performed in order to demonstrate that the beam is able to reproduce the measured dose distributions as expected by design. Secondly and to validate the commissioned beam model, calculated and measured dose distributions in water were compared for different pMLC shaped field sizes (2 x 2, 5 x 5, 10 x 10 cm^2) at SSDs ranging from 70 to 100 cm for electron beam energies ranging from 6 to 22 MeV.

Finally, a clinically realistic sternum case is considered as validation for the commissioned beam model. For this purpose, an Alderson anthropomorphic phantom is used and a CT scan from the chest part including the sternum is performed. The contours of the clinical target volume (CTV), the planning target volume (PTV) and structures of organs at risk, that is lungs and heart, from a clinical case are converted to the Alderson phantom to obtain a realistic situation. A dose of 30 Gy in 10 fraction was prescribed to the median dose of the PTV. Electron beams were manually setup utilizing a 22 MeV electron beam for this sternum case at two different SSDs of 75 and 96 cm. Applying an SSD = 75 cm demonstrates a short but still realistic SSD, while an SSD = 96 cm demonstrates a use case in which the iso-center corresponds with the iso-center used for image guided setup. Since due to in-air scatter of the electrons degrades the penumbra of the electron beam, reduced SSDs are advantageous (Klein *et al.*, 2008). The dose distributions for the pMLC shaped electron field are calculated using the commissioned beam model together with the eMC-2020 dose calculation

algorithm at both SSDs. During dose delivery in the developer mode of a TrueBeam equipped with a M120 pMLC, dose distributions using radiochromic films were measured in two transversal planes of the Alderson phantom per SSD. For this purpose, the scanned films were corrected for lateral scanner response artefacts (Lewis and Chan, 2015). A triple channel calibration was used to convert the scanned values to absolute dose along with the one-scan protocol (Micke *et al.*, 2011; Lewis *et al.*, 2012). The red color channel was used for the comparison of the four measured dose distributions with the corresponding calculated dose distributions by means of gamma passing rates. Gamma criteria of 3% (global) and 2 mm, 2% (global) and 2 mm as well as 1% (global) and 2 mm each with a threshold of 10% were used.

3. Results

3.1. Commissioning

The auto-commissioning was successfully implemented and applied for all available energies of the eight TrueBeam systems. Instead of the manual commissioning taking up to several days of calculation time and several hours of user time, the auto-commissioning is carried out in a few minutes for a single TrueBeam system.

Initially, all of the collected measurement data were reviewed. The analysis of measured lateral dose profiles at a depth of 1 cm in water in crossline and inline directions identified a systematic lateral offset of the dose profiles in inline direction of all the TrueBeam systems considered in this work. This lateral offset is different for different electron beam energies and most pronounced for high electron beam energies and an offset of up to about 2 mm at SSD = 90 cm was determined and is included optionally in the auto-commissioning process.

The first step in the auto-commissioning part is the construction of a two-dimensional fluence distribution for the main electron source and Figure 4 shows examples of such measurements and fluence profiles along with the resulting two-dimensional fluence distributions for two different electron beam energies. Thereby the measured fluence distributions were normalized to one on the central axis.

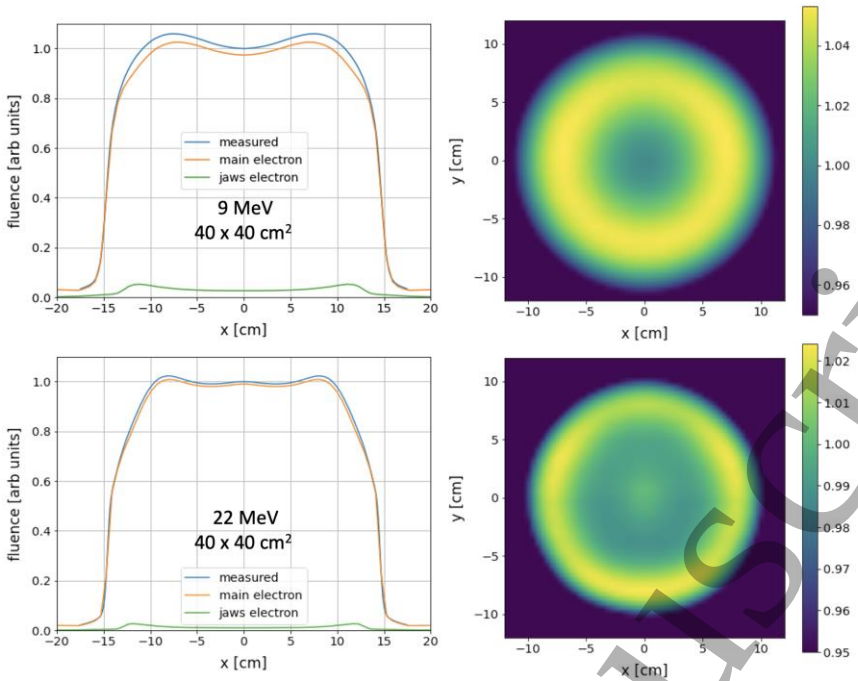

Figure 4. Measured crossline in-air profiles in the sampling plane for two different beam energies are shown on the left together with the fluence for the electrons from the jaw source as determined by BEAMnrc MC simulations and the fluence distribution of the main electron source determined as the difference between the measured and the electron fluence from the jaws. The colour coded two-dimensional fluence distribution for the main electron source for these beam energies constructed based on the in-air measured profiles are shown on the right. These fluence distributions are used in the sampling process of the beam model. Data shown for the Millennium-1 system.

During the auto-commissioning the focus position f and the standard deviation σ_f of the main source associated with the spot size are determined which is illustrated in Figure 5. Both parameters are determined independently from each other. The depth dose curves at SSD = 70 cm with the MLC fully retracted match measurements within 1% for all settings of f, as expected. As illustrated in Figure 5 there is a strong sensitivity of the output for the different settings of σ_f at the field size of 2 x 2 cm^2, which is also increasing for increasing electron beam energy. The resulting depth dose curves by means of interpolation is shown to match the corresponding measurements.

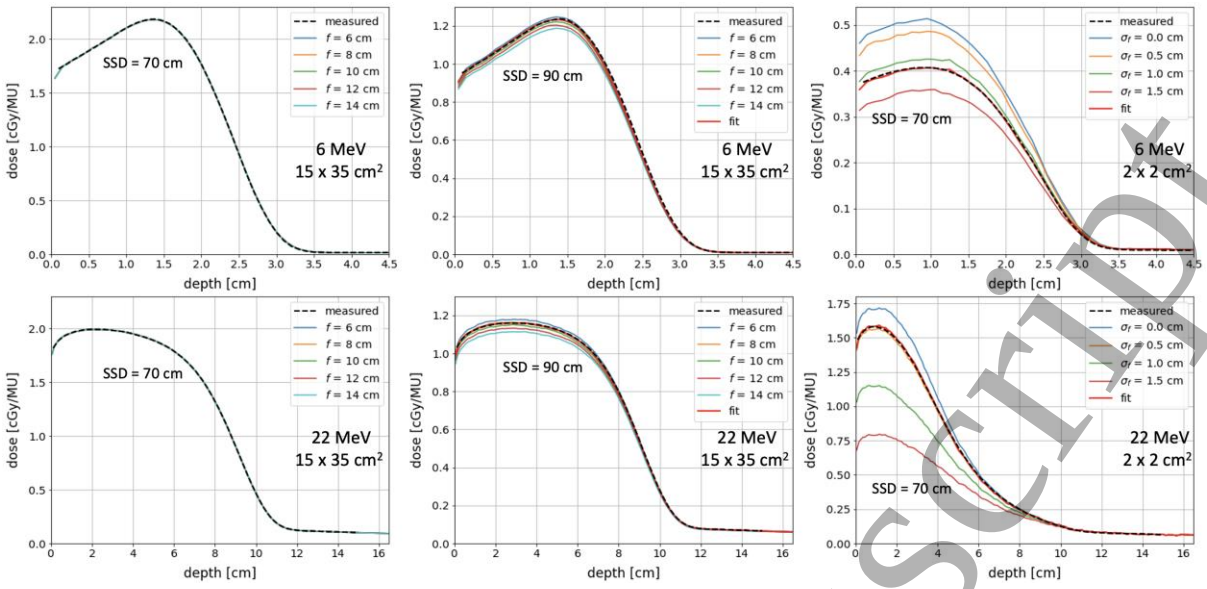

Figure 5. Illustration of the determination of the position of the focus *f* and the sigma σ_f of the main source as described in the auto-commissioning part (cf. section 2.4.) for two electron beam energies. The tuning process is designed to match depth dose curves at SSD = 70 cm (used as sampling plane in this case). To also match the measured depth dose curve at SSD = 90 cm the used focus position is interpolated. Applying the final value of the focus position, the measured depth dose curve for the field size of 2 x 2 cm^2 (at iso-center) is matched with calculated depth dose by interpolation of σ_f. Data shown for the Millennium-3 system.

Table 2 presents the resulting final values for the tuning parameters of the locations of the focus *f*, the sigma of the Gaussian shaped intensity distribution σ_f as well as the jaw-fraction for the different electron beam energies for the TrueBeam systems equipped with the M120 pMLC.

Table 2. Overview of the resulting electron beam model parameter focus *f*, sigma σ_f and jaw-fraction per electron beam energy of the auto-commissioning part for all TrueBeam system equipped with the Millennium 120 pMLC. Note, that for 16 and 20 MeV only one system was available.

Tuning Parameter	6 MeV	9 MeV	12 MeV	15 MeV	16 MeV	18 MeV	20 MeV	22 MeV
Focus *f* [cm] mean (min, max)	8.5 (7.2, 9.8)	8.0 (7.0, 8.8)	9.4 (8.8, 9.9)	8.4 (8.0, 8.8)	8.2	8.1 (7.7, 8.6)	8.5	8.3 (8.1, 8.5)
Sigma σ_f [cm] mean (min, max)	1.26 (1.14, 1.40)	0.63 (0.59, 0.69)	0.52 (0.49, 0.57)	0.50 (0.48, 0.55)	0.46	0.45 (0.42, 0.48)	0.44	0.42 (0.41, 0.44)
Jaw-fraction [%] mean (min, max)	4.1 (2.8, 5.1)	6.8 (6.3, 7.4)	6.1 (5.6, 6.7)	5.2 (4.9, 5.7)	5.4	5.0 (4.4, 5.9)	5.2	5.2 (5.0, 5.4)

Over all electron beam energies and TrueBeam systems, the variation of the focus position is within 3.5 cm, with the largest system to system variation for the 6 MeV electron beam energy. Although the focus positions are around the locations of the electron scattering foil systems in the linear accelerator head, there is no clear correlation with the specific electron scattering foils used for the different electron beam energies. While there is no clear dependency for the focus position and jaw-fraction as

a function of electron beam energy, the values for sigma decrease for increasing electron beam energy. In addition, the values for sigma are consistent and within 0.3 cm for the different TrueBeam systems and all electron beam energies and within 0.1 cm for the individual electron beam energies, except for the 6 MeV electron beam energy. The value for σ_f as well as its variation of within 0.25 cm for the 6 MeV beam is substantially larger compared to the remaining electron beam energies and might be due to the increase of in-air scatter at the low electron energy level. The corresponding values for the TrueBeam system equipped with the HDMLC are shown in Table 3.

Table 3. Overview of the resulting electron beam model parameter focus *f*, sigma σ_f and jaw-fraction per electron beam energy of the auto-commissioning part for the TrueBeam system equipped with the high-definition pMLC.

Tuning Parameter	6 MeV	9 MeV	12 MeV	16 MeV	20 MeV
Focus *f* [cm] mean	9.4	9.0	10.4	8.6	8.2
Sigma σ_f [cm] mean	1.27	0.69	0.55	0.49	0.41
Jaw-fraction [%] mean	1	6.1	8.1	7.1	6.2

3.2. Validation

As a first validation of the completely commissioned beam model, calculations of the dose distributions for those situations used during the commission are performed and some results of this dosimetric comparison are shown in Figure 6 in units of cGy/MU. Dose calculations in water using the fully commissioned beam model are able to match with the corresponding dose measurements generally within 1% for all situations considered.

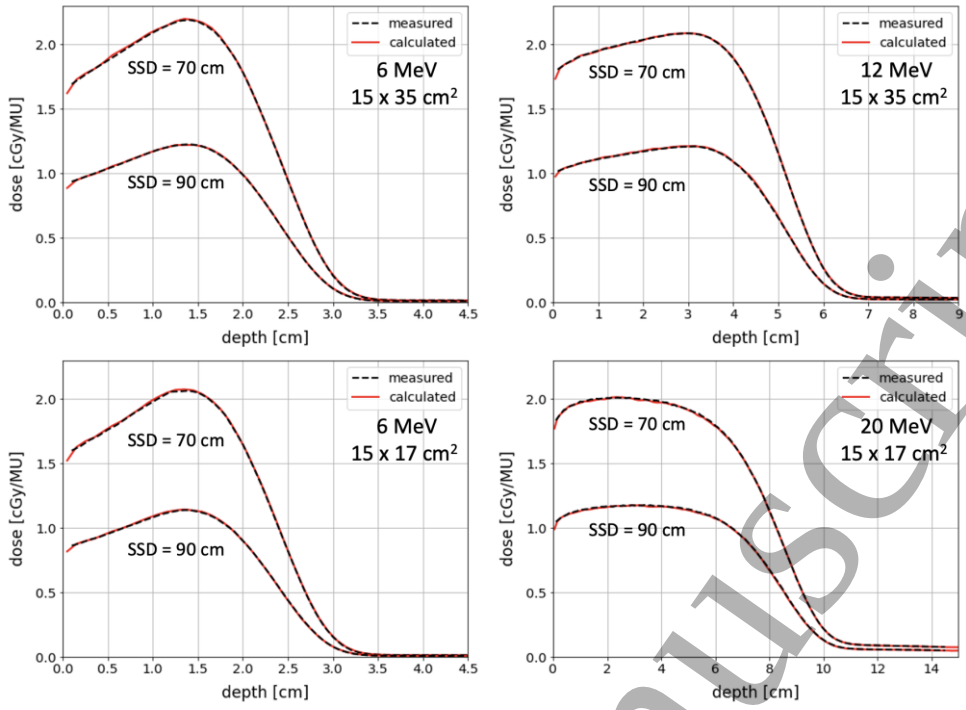

Figure 6. Comparison of measured and calculated absolute depth dose curves in water for different beam energies and field sizes of 15 x 35 cm^2 (upper row) and 15 x 17 cm^2 (lower row) of TrueBeam systems equipped with the Millennium 120 pMLC and the high-definition pMLC, respectively. The sampling plane is located at SSD = 70 cm. The agreement between measured and calculated dose values is below 1%. Data shown for the Millennium-6 system (upper row) and for the HDMLC-1 system (lower row).

The next level of validation includes comparisons of measured and calculated dose distributions in water for situations that were not used during the auto-commissioning. Some validation results with depth dose curves and lateral dose profiles are exemplarily shown in Figure 7 and Figure 8 for TrueBeam systems equipped with the M120 and with the HDMLC, respectively.

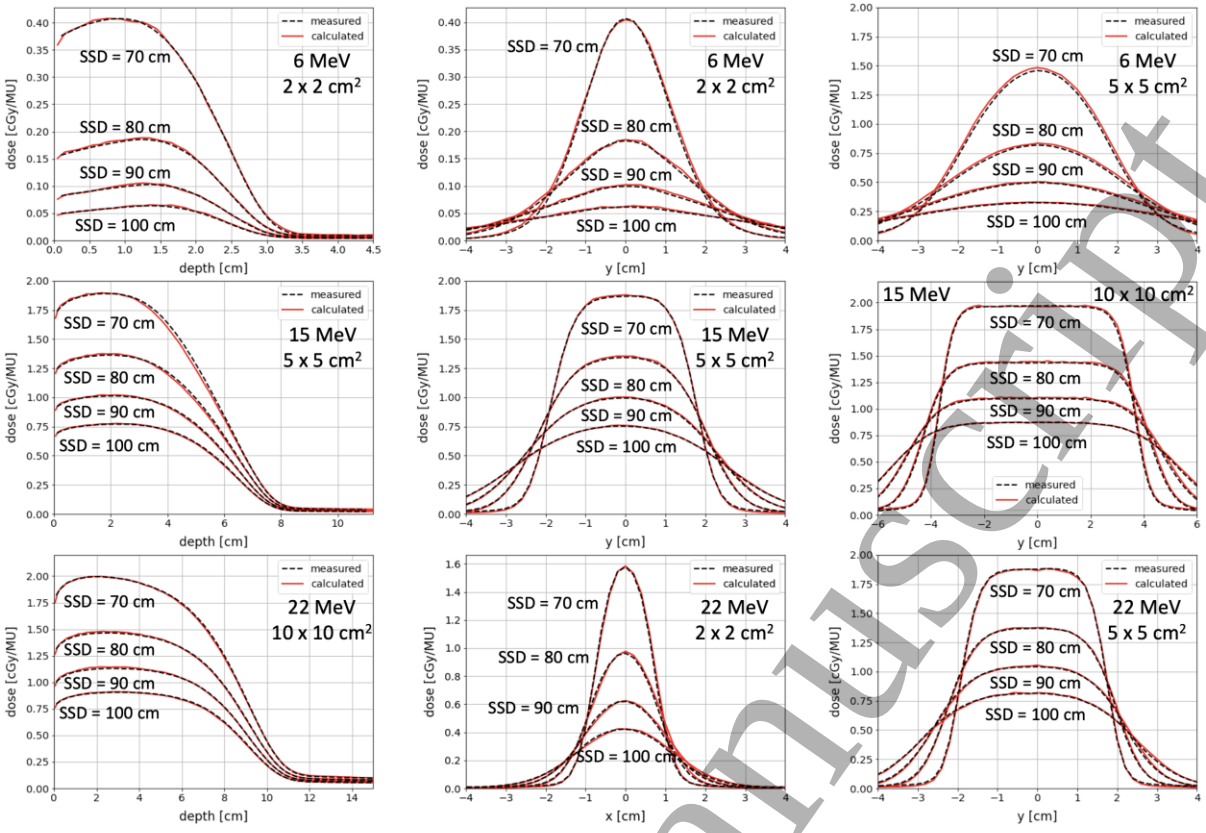

Figure 7. Examples of validation results by means of comparisons of measured and calculated absolute dose distributions for different pMLC shaped field sizes (at iso-center), SSDs and electron beam energies for a TrueBeam system equipped with Millennium 120 pMLC. The shown lateral dose profiles are at a depth of 1 cm in water. Data shown for the Millennium-3 system.

Note that all these comparisons are performed in absolute dose units over a large range of field sizes and SSDs. Overall, measured and calculated dose distributions agree generally within 3% of maximum dose or 2 mm distance to agreement for all TrueBeam systems considered.

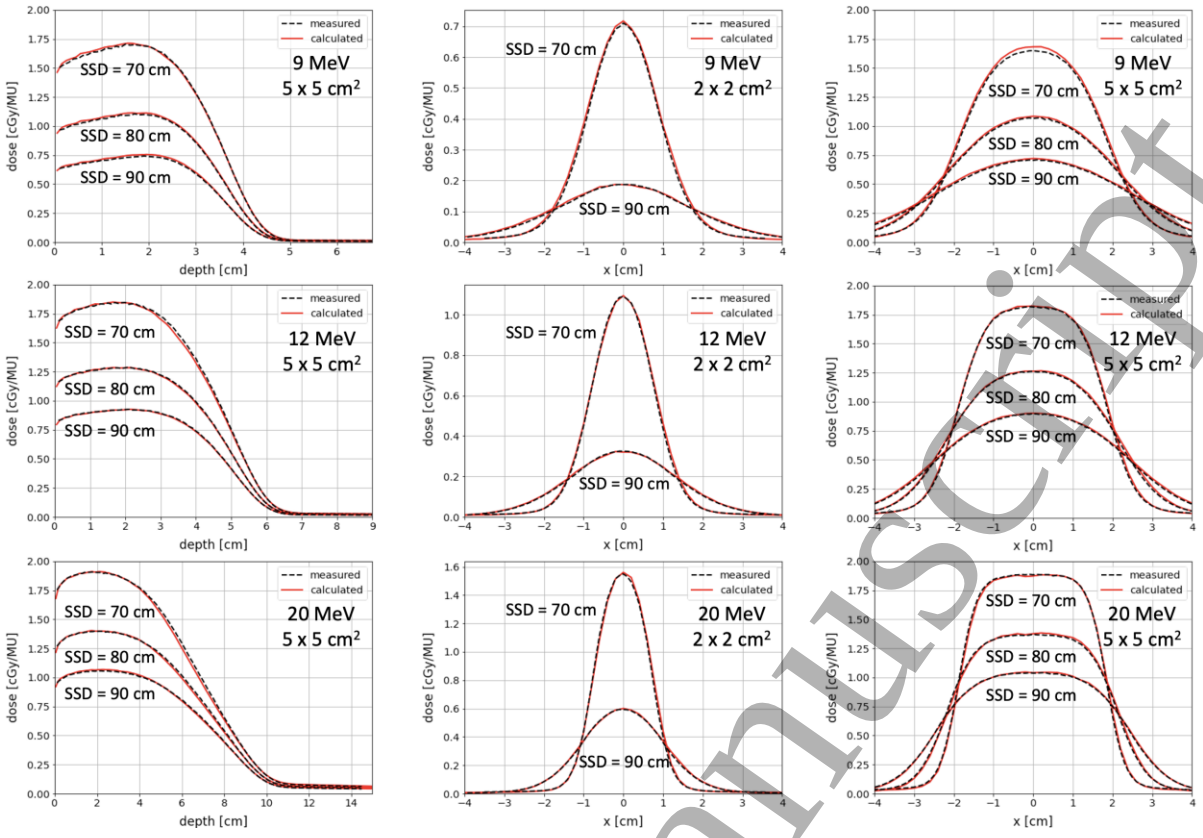

Figure 8. Examples of validation results by means of comparisons of measured and calculated absolute dose distributions for different pMLC shaped field sizes (at iso-center), SSDs and electron beam energies for TrueBeam systems equipped with high-definition pMLC. The shown lateral dose profiles are at a depth of 1 cm in water. Data shown for the HDMLC-1 system.

Finally, Figure 9 presents an example validation of the comparison of film measured and calculated dose distributions for the sternum case by means of gamma analysis using 3% (global) and 2 mm criteria with a threshold of 10%. The gamma passing rates for the two situations were 99% (both films) for dose delivery at SSD = 96 cm and 99% and 96% for dose delivery at SSD = 75 cm considered using the criteria mentioned above. When using the 2% instead of the 3% criterion the gamma passing rate were 97% (both films) for dose delivery at SSD = 96 cm and 99% and 93% for dose delivery at SSD = 75 cm. Using the 1% instead of the 3% criterion the gamma passing rate were 95% and 92% for dose delivery at SSD = 96 cm and 96% and 89% for dose delivery at SSD = 75 cm.

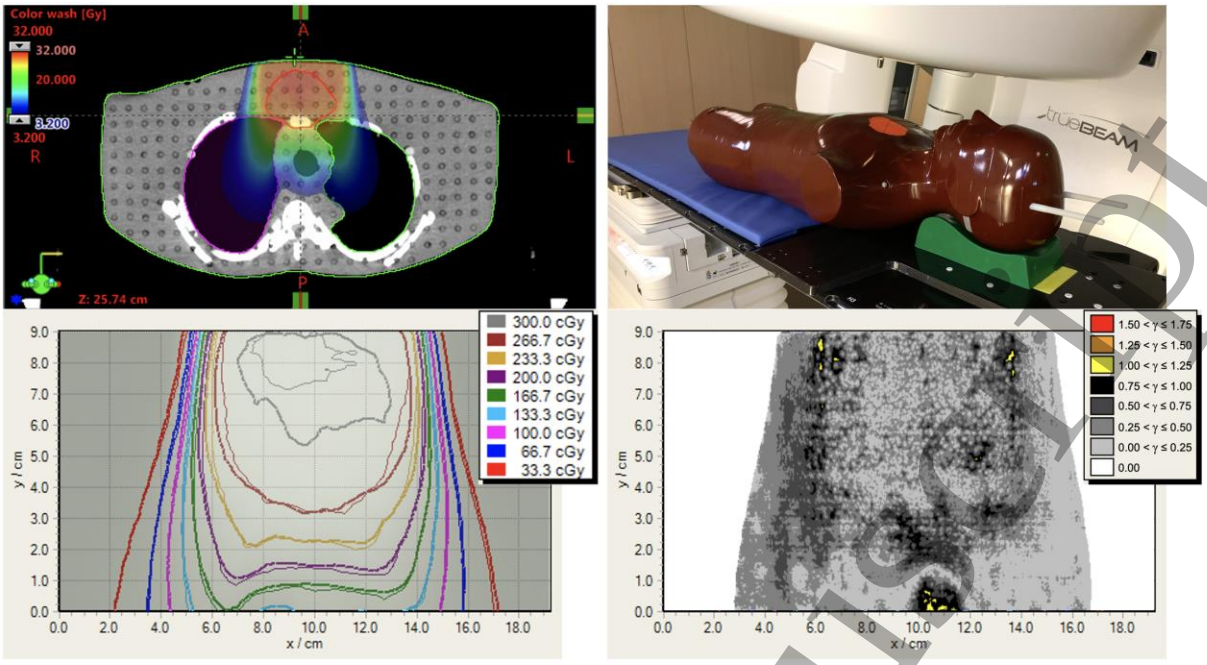

Figure 9. The upper row shows the dose distribution (left) and the setup (right) for the sternum case of the Alderson phantom at an SSD of 75 cm. On the bottom left the iso-dose comparison of measured (thin lines) and calculated (thick lines) dose distributions for one slice at an SSD of 75 cm is depicted. The corresponding gamma distribution leads to 99% passing rate for 3% (global) and 2 mm criteria with a 10% threshold (lower right).

4. Discussion and conclusions

This work presents a newly developed auto-commissioning procedure of a MC based beam model for pMLC shaped electron beams applicable for TrueBeam systems equipped with a M120 or an HDMLC. The commissioned beam model reproduces the electron beam characteristics leading to accurate dose distributions for a large range of SSDs, field sizes and electron beam energies ranging from 6 to 22 MeV. This was demonstrated for in total eight TrueBeam systems. It is important to mention that the enormous computational effort spent in the pre-determined MC simulations (cf. section 2.2) has to be done only once and is then applicable for all consecutively performed auto-commissioning of other TrueBeam systems. Hence, the application of the proposed procedure does not require any specific MC expertise for the auto-commissioning. In addition, no information of the beam defining system of the treatment unit or knowledge on how to generate the pre-determined data is needed by the user. The obtained database allows the auto-commissioning of the individual TrueBeam systems in a few minutes, while previously applied manual procedures needed several days of computation time along with hours for the user. The resulting accuracy when compared with

measurements corresponds at least to the level of agreement achieved for the manual procedure as shown by Mueller *et al.* (2018a). Other studies achieved agreement between measured and calculated percentage depth dose curves and lateral dose profiles within mainly 2% or 2 mm (Jin *et al.*, 2008; Klein *et al.*, 2008; Mihaljevic *et al.*, 2011; Henzen *et al.*, 2014c; Lloyd *et al.*, 2016). However, these studies compared relative dose distributions for at most two SSDs, while in this study absolute dose distributions over a larger range of SSDs are considered. Some small remaining dose differences observed in the validation as for example shown in Figures 6 and 7 might be due to uncertainties in the measurements such as setup uncertainties. In addition, also the beam model itself includes approximations and further improvements could reduce these remaining dose differences. Another advantage of the developed auto-commissioning procedure is that only two in-air dose profiles and four depth dose curves for the commissioning of one electron beam energy have to be acquired by the user with an additional lateral dose profile in order to determine the systematic lateral shift as discussed below. This is reduced compared to applicator-based electron radiotherapy, in which for each energy-applicator combination a set of dose measurements is needed (Cygler *et al.*, 2004; Ding *et al.*, 2006; Fix *et al.*, 2013; Huang *et al.*, 2019). For example, typically two to three days are needed to perform all commissioning measurements (including optional measurements) for a total of six electron beam energies for the electron MC algorithm in Eclipse (Varian Medical Systems, Palo Alto, CA). This can be reduced to one day for the commissioning measurements (including optional measurements) when using the proposed auto-commissioning.

When evaluating the different sets of measurements, a systematic shift of the lateral dose profiles in inline direction was observed. The larger the electron beam energy, the larger was the shift in the dose distribution reaching about 2 mm for the largest electron beam energy of 22 MeV considered in this work. This offset can be determined by means of a dose measurement and included optionally in the auto-commissioning process by either providing a value of this offset by the user or by providing a lateral dose profile acquired as described in the following. First the detector has to be aligned to the central beam axis using a 5 x 5 cm^2 pMLC shaped field of a photon beam, assuming a centered beam alignment for photon beams. Note that this alignment procedure should also be used for the

commissioning and validation measurements in order to avoid a misalignment due to the lateral offset in electron beams. Using this aligned detector position, the lateral dose profile in water in inline direction for a 5 x 5 cm^2 pMLC shaped field is measured at a depth of 1 cm in water at SSD = 90 cm. Since the pMLC for a collimator angle of 0° is not symmetric in the inline direction (bottle shaped pMLC leaves), a collimator rotation of 90° or 270° is suggested to be applied in order to shape the field by the rounded leaf ends of the pMLC. A lateral shift in inline direction can then be determined as the difference between the central beam axis and the center of the measured lateral dose profile. We hypothesize that the reason for such lateral shifts might be a combination of the impact of the fringe magnetic field from the bending magnet and a lateral offset of the focus location on the scattering foil (O'Shea *et al.*, 2011a). The auto-commissioning procedure allows to include this shift by counter-shifting the main source in the beam model accordingly. The impact of this behavior is illustrated Figure 10 showing comparisons of measured and calculated lateral dose profiles for different pMLC shaped field sizes, different SSDs and an electron beam energy of 22 MeV. This demonstrates the capability of the beam model and the auto-commissioning procedure to take such a shift into account.

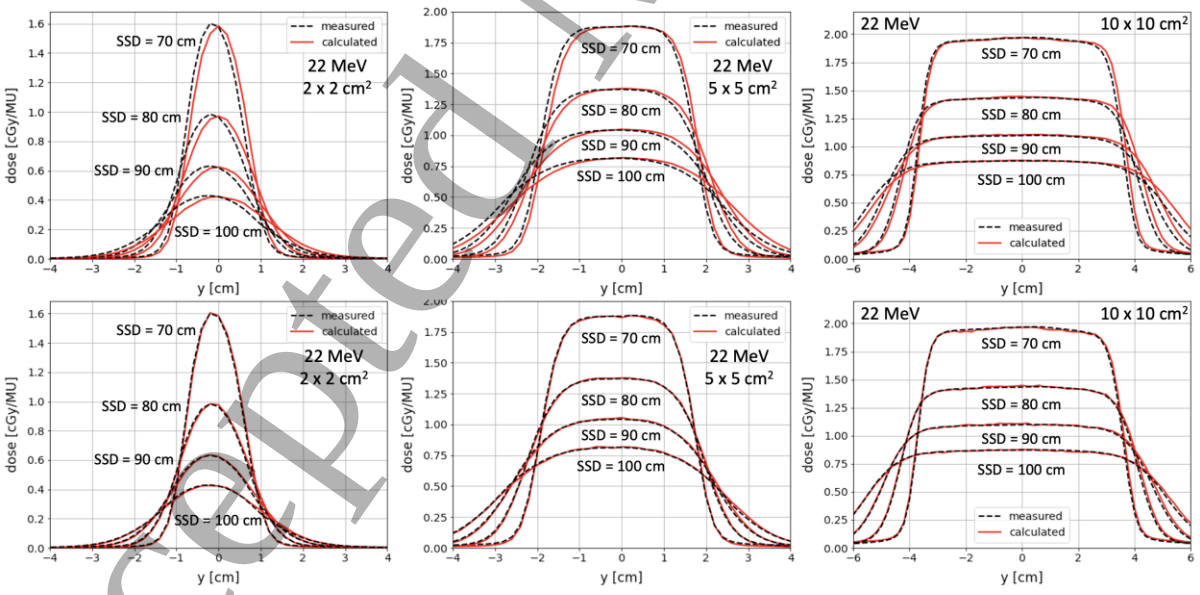

Figure 10. Validation results when ignoring (upper row) and considering (bottom row) the TrueBeam specific lateral shift of the beam in inline direction for the auto-commissioning of the beam models. Comparisons shown for measured and calculated lateral absolute dose profiles at a depth of 1 cm in water for different pMLC shaped field sizes (at iso-center) and SSDs for a 22 MeV electron beam energy. Data shown for the Millennium-3 system.

The proposed beam model explicitly simulates the radiation transport in the pMLC. However, compared to photon beams the geometrical implementation of the pMLC for electron beams was substantially simplified without impacting the accuracy of the calculated dose distribution. For example, the mechanical guides were omitted. The simplification improves the computational efficiency of the MC transport through the pMLC by a factor of about 100 to 300 depending on the energy and the pMLC type.

In this study, an auto-commissioning procedure was developed for TrueBeam systems. However, it is assumed that the developed methodology of the procedure would also work for different treatment units that offer electron treatment fields. Nonetheless, information of the beam defining system is necessary in order to generate the corresponding configuration data.

The newly developed auto-commissioning process allows an efficient commissioning of an MC electron beam model for TrueBeam systems equipped with an M120 or an HDMLC without dedicated MC expertise by the user. Measured and calculated dose distributions agree generally within 3% of maximum dose or 2 mm distance to agreement over a large range of SSDs and field sizes. This auto-commissioning procedure enables the dose calculation of pMLC shaped electron fields and thus supports the usage of more advanced techniques in electron radiation therapy such as MERT as well as different kinds of MBRT.

Acknowledgments

This work was supported by Varian Medical Systems. Calculations were performed on UBELIX (http://www.id.unibe.ch/hpc), the HPC cluster at the University of Bern. We would like to thank C. Chatelain, D. Frauchiger, L. Mikroutsikos, Dr H. Neuenschwander and R. Seiler for providing commissioning and validation measurements of their TrueBeam systems.

Appendix

This appendix provides more details about the improvements implemented in eMC for the eMC-2020 version used in this work for dose calculations. First, during the local MC simulation of the spheres with different materials it was observed that the energy and direction of the secondary particles

leaving the sphere are correlated (see Figure A1 left). When binning these particles on the energy axis a mean direction angle ϑ_{mean} can be determined, as shown as red dots in Figure A1 (left). Dividing the direction distribution in each energy bin by the corresponding mean value ϑ_{mean} leads to the distribution in Figure A1 (middle), that is the data is now presented with a substantially reduced correlation.

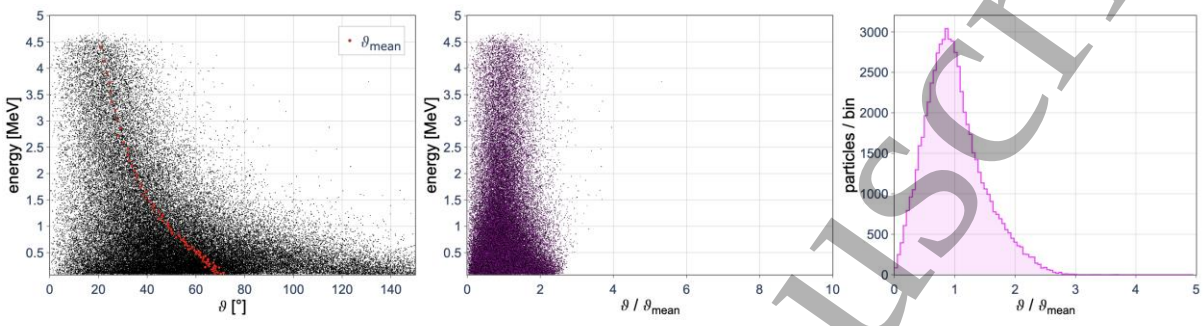

Figure A1. Energy-direction scatter plot for secondary particles (left) resulting from scored data of the local simulation (water sphere with 4 mm diameter for 10 MeV electrons). Energy-binning with bins including the same number of particles lead to mean theta values indicated by the red dots in the scatter plot on the left. Normalizing all particles within an energy bin by the obtained mean theta value leads to the distribution shown in the scatter plot on the right with substantially reduced correlation.

This distribution is then used in the global simulation to reproduce the energy-direction correlation for the secondary particles. For this purpose, all particles are used to determine a one-dimensional distribution as shown in Figure A1 (right), from which a value is sampled. After sampling the energy of the secondary particle, the sampled relative $\vartheta/\vartheta_{mean}$ value is multiplied by the ϑ_{mean} value of the corresponding energy bin. Thus, the correlated distribution shown in Figure A1 (left) is reproduced. The impact of this specific improvement is exemplarily shown in Figure A2.

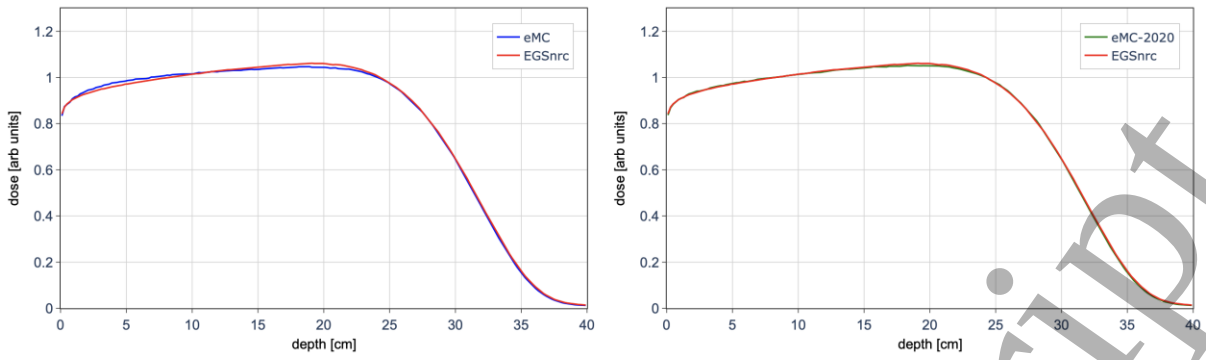

Figure A2. Impact of the correlated energy-direction sampling for the secondary particles on the dose distribution for electrons with an energy of 22 MeV in lung resulting in an improved agreement with full EGSnrc dose calculation. Left: without correlated sampling in eMC; Right: correlated sampling enabled in eMC-2020.

The second improvement considers the energy deposition of the primary electron. For this purpose, the sphere in the local simulation was sliced and the energy deposition in each slice was scored. This information can then be used during the energy deposition in the global simulation. The impact of this second specific improvement is exemplarily shown in Figure A3.

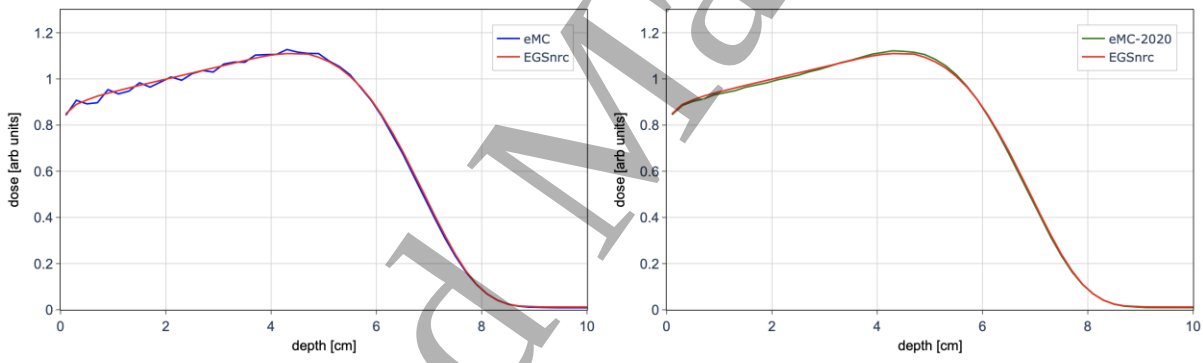

Figure A3. Impact of the modified energy deposition of the primary electron on the dose distribution for electrons with an energy of 16 MeV in water resulting in an improved agreement with full EGSnrc dose calculation. Left: without modified energy deposition in eMC; Right: modified energy deposition enabled in eMC-2020.

Furthermore, an additional material was included in the database, that is lung with a density of 0.1 g/cm^3 (lung light) was included between air and lung with density of 0.3 g/cm^3. Overall, the accuracy of the dose calculation was improved when compared eMC-2020 with eMC and EGSnrc, where the latter was used as benchmark. This improvement is exemplarily demonstrated in Figure A4.

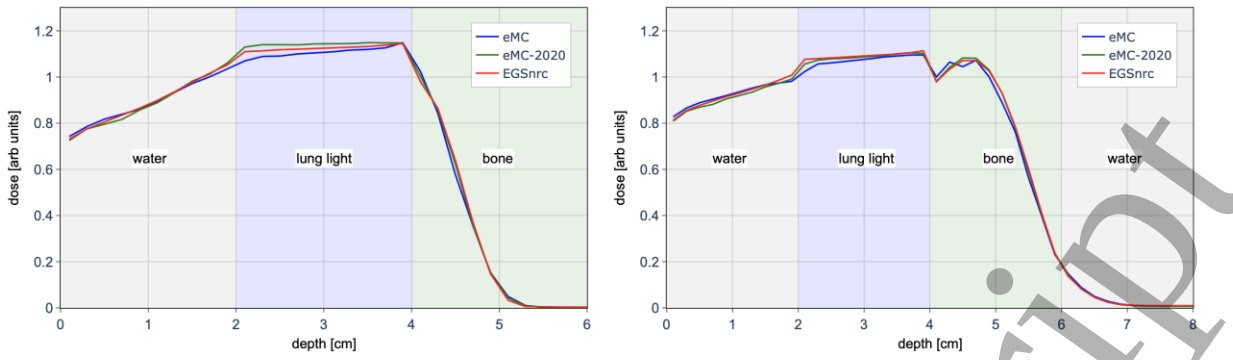

Figure A4. Comparison of dose distributions in an inhomogeneous phantom using the eMC, the improved eMC-2020 version and EGSnrc for dose calculation of mono-energetic electrons with an energy of 8 MeV (left) and 12 MeV (right). The eMC-2020 version shows an improved agreement with EGSnrc compared to eMC.

Finally, a dedicated air transport was developed, which is specifically applied for the air transport between the beam reconstruction plane and the patient, to further improve the efficiency of eMC-2020 compared to EGSnrc. This dedicated air transport takes multiple scattering into account, but no energy deposition is scored, no secondary particles are generated and larger spheres of up to a diameter of 4 cm are included in the database of eMC-2020.

References

Al-Yahya K, Schwartz M, Shenouda G, Verhaegen F, Freeman C and Seuntjens J 2005 Energy modulated electron therapy using a few leaf electron collimator in combination with IMRT and 3D-CRT: Monte Carlo-based planning and dosimetric evaluation *Medical physics* **32** 2976-86

Al-Yahya K, Verhaegen F and Seuntjens J 2007 Design and dosimetry of a few leaf electron collimator for energy modulated electron therapy *Medical physics* **34** 4782-91

Alexander A, DeBlois F and Seuntjens J 2010 Toward automatic field selection and planning using Monte Carlo-based direct aperture optimization in modulated electron radiotherapy *Physics in medicine and biology* **55** 4563-76

Ali O A, Willemse C A, Shaw W, O'Reilly F H and du Plessis F C 2011 Monte carlo electron source model validation for an Elekta Precise linac *Medical physics* **38** 2366-73

Bortfeld T R, Kahler D L, Waldron T J and Boyer A L 1994 X-ray field compensation with multileaf collimators *Int J Radiat Oncol Biol Phys* **28** 723-30

Boyer A L, et al. 2001. Basic applications of multileaf collimators *Med Phys AAPM Report* No 72 (Alexandria, VA: AAPM) (https://aapm.org/pubs/reports/RPT_72.pdf)

Brewster L, Mohan R, Mageras G, Burman C, Leibel S and Fuks Z 1995 Three dimensional conformal treatment planning with multileaf collimators *Int J Radiat Oncol Biol Phys* **33** 1081-9

Convery D J and Rosenbloom M E 1992 The generation of intensity-modulated fields for conformal radiotherapy by dynamic collimation *Physics in medicine and biology* **37** 1359-74

Cygler J E, Daskalov G M, Chan G H and Ding G X 2004 Evaluation of the first commercial Monte Carlo dose calculation engine for electron beam treatment planning *Medical physics* **31** 142-53

Cygler J E, et al. 2005 Clinical use of a commercial Monte Carlo treatment planning system for electron beams *Physics in medicine and biology* **50** 1029-34

Ding G X, Cygler J E, Yu C W, Kalach N I and Daskalov G 2005 A comparison of electron beam dose calculation accuracy between treatment planning systems using either a pencil beam or a Monte Carlo algorithm *Int J Radiat Oncol Biol Phys* **63** 622-33

Ding G X, Duggan D M, Coffey C W, Shokrani P and Cygler J E 2006 First macro Monte Carlo based commercial dose calculation module for electron beam treatment planning--new issues for clinical consideration *Physics in medicine and biology* **51** 2781-99

du Plessis F C, Leal A, Stathakis S, Xiong W and Ma C M 2006 Characterization of megavoltage electron beams delivered through a photon multi-leaf collimator (pMLC) *Physics in medicine and biology* **51** 2113-29

Edimo P, Clermont C, Kwato M G and Vynckier S 2009 Evaluation of a commercial VMC++ Monte Carlo based treatment planning system for electron beams using EGSnrc/BEAMnrc simulations and measurements *Phys Med* **25** 111-21

Eldib A, Jin L, Li J and Ma C M 2013 Feasibility of replacing patient specific cutouts with a computer-controlled electron multileaf collimator *Physics in medicine and biology* **58** 5653-72

Engel K and Gauer T 2009 A dose optimization method for electron radiotherapy using randomized aperture beams *Physics in medicine and biology* **54** 5253-70

Fix M K, et al. 2013 Generalized eMC implementation for Monte Carlo dose calculation of electron beams from different machine types *Physics in medicine and biology* **58** 2841-59

Fix M K, Frei D, Volken W, Neuenschwander H, Born E J and Manser P 2010 Monte Carlo dose calculation improvements for low energy electron beams using eMC *Physics in medicine and biology* **55** 4577-88

Fix M K, et al. 2018 Part 1: Optimization and evaluation of dynamic trajectory radiotherapy *Medical physics*

Fragoso M, Pillai S, Solberg T D and Chetty I J 2008 Experimental verification and clinical implementation of a commercial Monte Carlo electron beam dose calculation algorithm *Medical physics* **35** 1028-38

Gauer T, Engel K, Kiesel A, Albers D and Rades D 2010 Comparison of electron IMRT to helical photon IMRT and conventional photon irradiation for treatment of breast and chest wall tumours *Radiotherapy and oncology : journal of the European Society for Therapeutic Radiology and Oncology* **94** 313-8

Ge Y and Faddegon B A 2011 Study of intensity-modulated photon-electron radiation therapy using digital phantoms *Physics in medicine and biology* **56** 6693-708

Guyer G, et al. 2022 Enabling non-isocentric dynamic trajectory radiotherapy by integration of dynamic table translations *Physics in medicine and biology* **67**

Heng V J, Serban M, Seuntjens J and Renaud M A 2021 Ion chamber and film-based quality assurance of mixed electron-photon radiation therapy *Medical physics* **48** 5382-95

Henzen D, et al. 2014a Beamlet based direct aperture optimization for MERT using a photon MLC *Medical physics* **41** 121711

Henzen D, et al. 2014b Forward treatment planning for modulated electron radiotherapy (MERT) employing Monte Carlo methods *Medical physics* **41** 031712

Henzen D, et al. 2014c Monte Carlo based beam model using a photon MLC for modulated electron radiotherapy *Medical physics* **41** 021714

Huang J Y, Dunkerley D and Smilowitz J B 2019 Evaluation of a commercial Monte Carlo dose calculation algorithm for electron treatment planning *Journal of applied clinical medical physics / American College of Medical Physics* **20**(6) 184-93

Jin L, et al. 2014 Measurement and Monte Carlo simulation for energy- and intensity-modulated electron radiotherapy delivered by a computer-controlled electron multileaf collimator *Journal of applied clinical medical physics / American College of Medical Physics* **15**(1) 4506

Jin L, et al. 2008 Dosimetric verification of modulated electron radiotherapy delivered using a photon multileaf collimator for intact breasts *Physics in medicine and biology* **53** 6009-25

Kaluarachchi M M, Saleh Z H, Schwer M L and Klein E E 2020 Validation of a Monte Carlo model for multi leaf collimator based electron delivery *Medical physics* **47** 3586-99

Kawrakow I and Rogers D W O 2002 The EGSnrc code system: Monte Carlo simulation of electron and photon transport *NRCC Repor PIRS-701* (Ottawa: Ionizing Radiation Standards, National Research Council of Canada)

Klein E E, Mamalui-Hunter M and Low D A 2009 Delivery of modulated electron beams with conventional photon multi-leaf collimators *Physics in medicine and biology* **54** 327-39

Klein E E, Vicic M, Ma C M, Low D A and Drzymala R E 2008 Validation of calculations for electrons modulated with conventional photon multileaf collimators *Physics in medicine and biology* **53** 1183-208

Leal A, et al. 2004 Monte Carlo simulation of complex radiotherapy treatments *Computing in Science & Engineering* **6** 60-8

Lewis D and Chan M F 2015 Correcting lateral response artifacts from flatbed scanners for radiochromic film dosimetry *Medical physics* **42** 416-29

Lewis D, Micke A, Yu X and Chan M F 2012 An efficient protocol for radiochromic film dosimetry combining calibration and measurement in a single scan *Medical physics* **39** 6339-50

Lloyd S A, Zavgorodni S and Gagne I M 2015 Comparison of measured Varian Clinac 21EX and TrueBeam accelerator electron field characteristics *Journal of applied clinical medical physics / American College of Medical Physics* **16** 193-201

Lloyd S A M, Gagne I M, Bazalova-Carter M and Zavgorodni S 2016 Validation of Varian TrueBeam electron phase-spaces for Monte Carlo simulation of MLC-shaped fields *Medical physics* **43** 2894-903

Lynch G R and Dahl O I 1991 Approximations to multiple Coulomb scattering *Nuclear Instruments and Methods in Physics Research Section B: Beam Interactions with Materials and Atoms* **58** 6-10

Micke A, Lewis D F and Yu X 2011 Multichannel film dosimetry with nonuniformity correction *Medical physics* **38** 2523-34

Mihaljevic J, Soukup M, Dohm O and Alber M 2011 Monte Carlo simulation of small electron fields collimated by the integrated photon MLC *Physics in medicine and biology* **56** 829-43

Mueller S, et al. 2018a Electron beam collimation with a photon MLC for standard electron treatments *Physics in medicine and biology* **63** 025017

Mueller S, et al. 2022 A hybrid column generation and simulated annealing algorithm for direct aperture optimization *Physics in medicine and biology* **67**

Mueller S, et al. 2018b Part 2: Dynamic mixed beam radiotherapy (DYMBER): Photon dynamic trajectories combined with modulated electron beams *Medical physics*

Neuenschwander H and Born E J 1992 A macro Monte Carlo method for electron beam dose calculations *Physics in medicine and biology* **37** 107-25

O'Shea T P, Foley M J and Faddegon B A 2011a Accounting for the fringe magnetic field from the bending magnet in a Monte Carlo accelerator treatment head simulation *Medical physics* **38** 3260-9

O'Shea T P, Ge Y, Foley M J and Faddegon B A 2011b Characterization of an extendable multi-leaf collimator for clinical electron beams *Physics in medicine and biology* **56** 7621-38

Ojala J, Kapanen M and Hyodynmaa S 2016 Full Monte Carlo and measurement-based overall performance assessment of improved clinical implementation of eMC algorithm with emphasis on lower energy range *Phys Med* **32** 801-11

Otto K 2008 Volumetric modulated arc therapy: IMRT in a single gantry arc *Medical physics* **35** 310-7

Palma B A, et al. 2012 Combined modulated electron and photon beams planned by a Monte-Carlo-based optimization procedure for accelerated partial breast irradiation *Physics in medicine and biology* **57** 1191-202

Pemler P, Besserer J, Schneider U and Neuenschwander H 2006 Evaluation of a commercial electron treatment planning system based on Monte Carlo techniques (eMC) *Zeitschrift fur medizinische Physik* **16** 313-29

Popple R A, et al. 2006 Comprehensive evaluation of a commercial macro Monte Carlo electron dose calculation implementation using a standard verification data set *Medical physics* **33** 1540-51

Renaud M A, Serban M and Seuntjens J 2017 On mixed electron-photon radiation therapy optimization using the column generation approach *Medical physics* **44** 4287-98

Renaud M A, Serban M and Seuntjens J 2019 Robust mixed electron-photon radiation therapy optimization *Medical physics* **46** 1384-96

Rogers D W O, Faddegon B A, Ding G X, Ma C-M, We J and Mackie T R 1995 BEAM: a Monte Carlo code to simulate radiotherapy treatment units *Medical physics* **22** 503-24

Salguero F J, Arrans R, Palma B A and Leal A 2010 Intensity- and energy-modulated electron radiotherapy by means of an xMLC for head and neck shallow tumors *Physics in medicine and biology* **55** 1413-27

Salguero F J, Palma B, Arrans R, Rosello J and Leal A 2009 Modulated electron radiotherapy treatment planning using a photon multileaf collimator for post-mastectomized chest walls *Radiotherapy and oncology : journal of the European Society for Therapeutic Radiology and Oncology* **93** 625-32

Skinner L, Fahimian B P and Yu A S 2019 Tungsten filled 3D printed field shaping devices for electron beam radiation therapy *PLoS One* **14** e0217757

Smyth G, Evans P M, Bamber J C and Bedford J L 2019 Recent developments in non-coplanar radiotherapy *Br J Radiol* **92** 20180908

Snyder J E, Hyer D E, Flynn R T, Boczkowski A and Wang D 2019 The commissioning and validation of Monaco treatment planning system on an Elekta VersaHD linear accelerator *Journal of applied clinical medical physics / American College of Medical Physics* **20**(1) 184-93

Surucu M, Klein E E, Mamalui-Hunter M, Mansur D B and Low D A 2010 Planning tools for modulated electron radiotherapy *Medical physics* **37** 2215-24

Vatanen T, Traneus E and Lahtinen T 2009 Comparison of conventional inserts and an add-on electron MLC for chest wall irradiation of left-sided breast cancer *Acta Oncol* **48** 446-51

Yu C X 1995 Intensity-modulated arc therapy with dynamic multileaf collimation: an alternative to tomotherapy *Physics in medicine and biology* **40** 1435-49